

Compute SNR-Optimal Analog-to-Digital Converters for Analog In-Memory Computing

Mihir Kavishwar and Naresh Shanbhag

Department of Electrical and Computer Engineering,
University of Illinois Urbana-Champaign, Urbana, IL 61801

Abstract—Analog in-memory computing (AIMC) is an energy-efficient alternative to digital architectures for accelerating machine learning and signal processing workloads. However, its energy efficiency is limited by the high energy cost of the column analog-to-digital converters (ADCs). Reducing the ADC precision is an effective approach to lowering its energy cost. However, doing so also reduces the AIMC’s computational accuracy thereby making it critical to identify the minimum precision required to meet a target accuracy. Prior works overestimate the ADC precision requirements by modeling quantization error as input-independent noise, maximizing the signal-to-quantization-noise ratio (SQNR), and ignoring the discrete nature of ideal pre-ADC signal. We address these limitations by developing analytical expressions for estimating the compute signal-to-noise ratio (CSNR), a true metric of accuracy for AIMCs, and propose CACTUS, an algorithm to obtain CSNR-optimal ADC parameters. Using a circuit-aware behavioral model of an SRAM-based AIMC in a 28 nm CMOS process, we show that for a 256-dimensional binary dot product, CACTUS reduces the ADC precision requirements by 3 b while achieving 6 dB higher CSNR over prior methods. We also delineate operating conditions under which our proposed CSNR-optimal ADCs outperform conventional SQNR-optimal ADCs.

Index Terms—analog in-memory computing, analog-to-digital converter, compute signal-to-noise ratio, optimal clipping criteria

I. INTRODUCTION

Analog in-memory computing (AIMC) is emerging as a promising architecture for the energy-efficient execution of matrix-vector multiplication (MVM) operations, which dominate modern machine learning and signal processing workloads [1]–[4]. AIMCs store large matrices in memory arrays, such as static random access memory (SRAM) [5]–[16] or embedded non-volatile memory (eNVM) [17]–[21]. MVM operations are performed by applying input vectors to memory arrays, which compute dot products in the analog domain using charge or current accumulation, followed by digitization through analog-to-digital converters (ADCs). By integrating memory and computation, AIMCs eliminate frequent data transfers between separate memory and processing units - a major energy bottleneck in traditional von Neumann architectures [22], [23]. However, this integration comes at the cost of significant ADC energy overhead. Fig. 1 shows that ADCs can account for up to 60% of the total energy consumption in state-of-the-art AIMCs today.

Lowering ADC precision reduces their energy cost [24], thereby improving AIMC’s energy efficiency. However, this also degrades AIMC’s computational accuracy, creating an

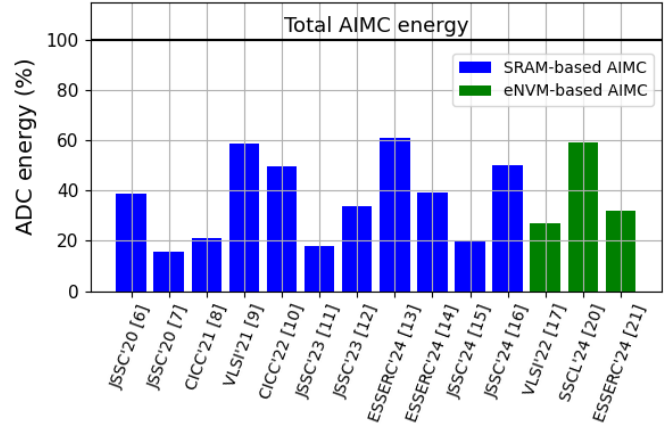


Fig. 1: ADC energy contribution in state-of-the-art analog in-memory computing (AIMC) ICs.

energy-accuracy trade-off. Therefore, there is much interest in determining the minimum ADC precision required in AIMCs to achieve a target computational accuracy, e.g. [25]–[29]. These works suffer from two deficiencies: 1) they estimate the AIMC’s minimum ADC precision requirements by maximizing the ADCs signal-to-quantization-noise ratio (SQNR) using it as a proxy for the computational accuracy of an AIMC; and 2) they model quantization errors as input-independent and the pre-ADC signal $V_{\text{pre-adc}}$ as Gaussian distributed. Our work shows that both deficiencies lead to a significantly pessimistic estimate of the minimum required ADC precision. Since ADC energy quadruples in the noise-dominated regime [24], [27], even a single bit reduction in ADC precision can be impactful in the overall energy efficiency of the AIMC.

In this paper, we determine the minimum ADC precision for AIMCs by: 1) maximizing the compute signal-to-noise ratio (CSNR) instead of SQNR. In doing so, we minimize the mean squared error between the ideal output of a digital dot product computation and that of the AIMC, i.e., the computational error, rather than the mean squared error between the input and output of an ADC as is done conventionally; and 2) we adopt a realistic AIMC model that assumes dependence between ADC quantization errors and its input, and treats the ADC input as a Gaussian mixture rather than a Gaussian. Fig. 2 illustrates the difference between the distributions of the ideal voltage-domain dot product (V_{ideal}) and the actual

pre-ADC signal $V_{\text{pre-adc}}$ on the bitlines. Note that $V_{\text{pre-adc}}$ is a Gaussian mixture obtained by the addition of Gaussian noise representing ADC thermal noise and other noise sources, to a discrete-valued random variable V_{ideal} whose distribution tends to be binomial, e.g., $\text{Bi}(N, 0.25)$ for an N -dimension dot product computation. Prior works approximate this type of Gaussian mixture with a Gaussian which leads to pessimistic results.

Our key contributions are summarized below:

- We propose CSNR-optimal ADCs for AIMCs and highlight how they differ from SQNR-optimal ADCs (Section III).
- We derive analytical expressions for CSNR and MSE_{dp} in AIMCs, assuming a Gaussian mixture model for the ADC input and input-dependent quantization errors (Theorems 1 and 2 in Section III).
- Based on Theorems 1 and 2, we formulate CACTUS, an algorithm to identify CSNR-optimal quantization thresholds given an ADC precision, and use it to determine the minimum ADC precision required to meet a target CSNR (Section III(C)).
- We demonstrate, using a circuit-aware behavioral model of an SRAM-based AIMC in 28 nm CMOS, that CACTUS outperforms conventional baselines by achieving higher CSNR with lower ADC precision, e.g., for a 256-dimensional binary dot product, CACTUS reduces the ADC precision requirements by 3 b while achieving 6 dB higher CSNR over prior methods.
- We delineate operating conditions under which our proposed CSNR-optimal ADCs outperform conventional SQNR-optimal ADCs.

An anonymized repository of our code can be found at: <https://github.com/mihirvk2/CSNR-optimal-ADC>. The rest of this paper is organized as follows. Section II reviews the background on conventional ADCs and introduces CSNR as the accuracy metric for AIMC. Section III presents a theoretical analysis of CSNR-optimal ADCs and the CACTUS algorithm. Section IV discusses the simulation setup and results across various AIMC design parameters. Section V concludes the paper.

II. BACKGROUND AND RELATED WORKS

A. Quantization Function in ADCs

For a fixed ADC precision (B_{adc}), the ADC is defined by its quantization function ($Q_{\mathbf{t}, \mathbf{r}}$), which maps a continuous analog input to a discrete quantization level:

$$M = 2^{B_{\text{adc}}} - 1 \quad (1)$$

$$Q_{\mathbf{t}, \mathbf{r}}(V_{\text{in}}) = \begin{cases} r_0 & , \text{ if } V_{\text{in}} < t_1 \\ r_k & , \text{ if } t_k \leq V_{\text{in}} < t_{k+1}, k \in \{1, 2, \dots, M\} \\ r_M & , \text{ if } V_{\text{in}} \geq t_M \end{cases} \quad (2)$$

where V_{in} represents the analog input to the ADC, $Q_{\mathbf{t}, \mathbf{r}}(\cdot) : \mathbb{R} \rightarrow \{r_0, r_1, \dots, r_M\}$ is the quantization function of the ADC

with precision B_{adc} , thresholds $\mathbf{t} = [t_1, \dots, t_M] \in \mathbb{R}^M$ with $t_1 \leq \dots \leq t_M$, and quantization levels $\mathbf{r} = [r_0, \dots, r_M] \in \mathbb{R}^{M+1}$ with $r_0 < t_1, t_k \leq r_k < t_{k+1} \forall k \in \{1, 2, \dots, M-1\}$, $r_M \geq t_M$. The quantization levels \mathbf{r} are digitally encoded in hardware.

In uniform ADCs, the quantization function in (2) is constrained to have uniformly spaced thresholds and quantization levels as follows:

$$\Delta_{\text{adc}} = \frac{t_M - t_1}{M - 1} \quad (3)$$

$$t_k = t_1 + (k - 1) \times \Delta_{\text{adc}} \forall k \in \{1, 2, \dots, M\} \quad (4)$$

$$r_k = t_1 + (k - 0.5) \times \Delta_{\text{adc}} \forall k \in \{0, 1, \dots, M\} \quad (5)$$

where Δ_{adc} is called the quantization step size of the ADC. The smallest and largest thresholds, t_1 and t_M , are also known as the *clipping thresholds*. Thus, quantization function of a uniform ADC can be completely expressed in terms of t_1 and t_M .

While in theory, non-uniform ADCs, i.e., ADCs with non-uniformly spaced quantization thresholds and levels are possible, such ADCs are difficult to design and their outputs cannot be processed using standard arithmetic blocks (adders and multipliers) due to the intrinsic non-linearity in the conversion process. Hence, in this paper, we focus on the commonly used uniform ADCs.

B. SQNR-optimal ADCs

The quantization process in an ADC results in a quantization error/noise given by:

$$q(V_{\text{in}}) = Q_{\mathbf{t}, \mathbf{r}}(V_{\text{in}}) - V_{\text{in}} \quad (6)$$

where $q(V_{\text{in}})$ represents the quantization error corresponding to the input signal V_{in} . The ADC's accuracy is measured using the signal-to-quantization-noise ratio (SQNR), defined as:

$$\text{SQNR} = \frac{\text{Var}(V_{\text{in}})}{\mathbb{E}[(Q_{\mathbf{t}, \mathbf{r}}(V_{\text{in}}) - V_{\text{in}})^2]} = \frac{\text{Var}(V_{\text{in}})}{\text{MSE}_{\text{q}}} \quad (7)$$

where V_{in} is a random variable representing the analog ADC input, $\text{Var}(\cdot)$ denotes variance, $\mathbb{E}[\cdot]$ denotes expected value, and MSE_{q} is the mean squared quantization error. Thus, maximizing SQNR is equivalent to minimizing MSE_{q} . For a given ADC precision B_{adc} , we define an SQNR-optimal ADC as the solution to the following optimization problem:

$$\begin{aligned} \{\mathbf{t}^*, \mathbf{r}^*\} &= \arg \max_{\mathbf{t}, \mathbf{r}} \text{SQNR} = \arg \min_{\mathbf{t}, \mathbf{r}} \text{MSE}_{\text{q}} \\ &= \arg \min_{\mathbf{t}, \mathbf{r}} \mathbb{E}[(Q_{\mathbf{t}, \mathbf{r}}(V_{\text{in}}) - V_{\text{in}})^2] \end{aligned} \quad (8)$$

where \mathbf{t}^* and \mathbf{r}^* are the thresholds and quantization levels of the SQNR-optimal ADC, respectively.

The Lloyd-Max (LM) algorithm [30], [31] is a well-established method for iteratively solving the unconstrained optimization problem in (8) to obtain the SQNR-optimal thresholds and quantization levels when the distribution of V_{in} is known. However, LM guarantees convergence only to a local minimum of MSE_{q} , making it SQNR-optimal only when the ADC input distribution has a single peak [32]. Additionally,

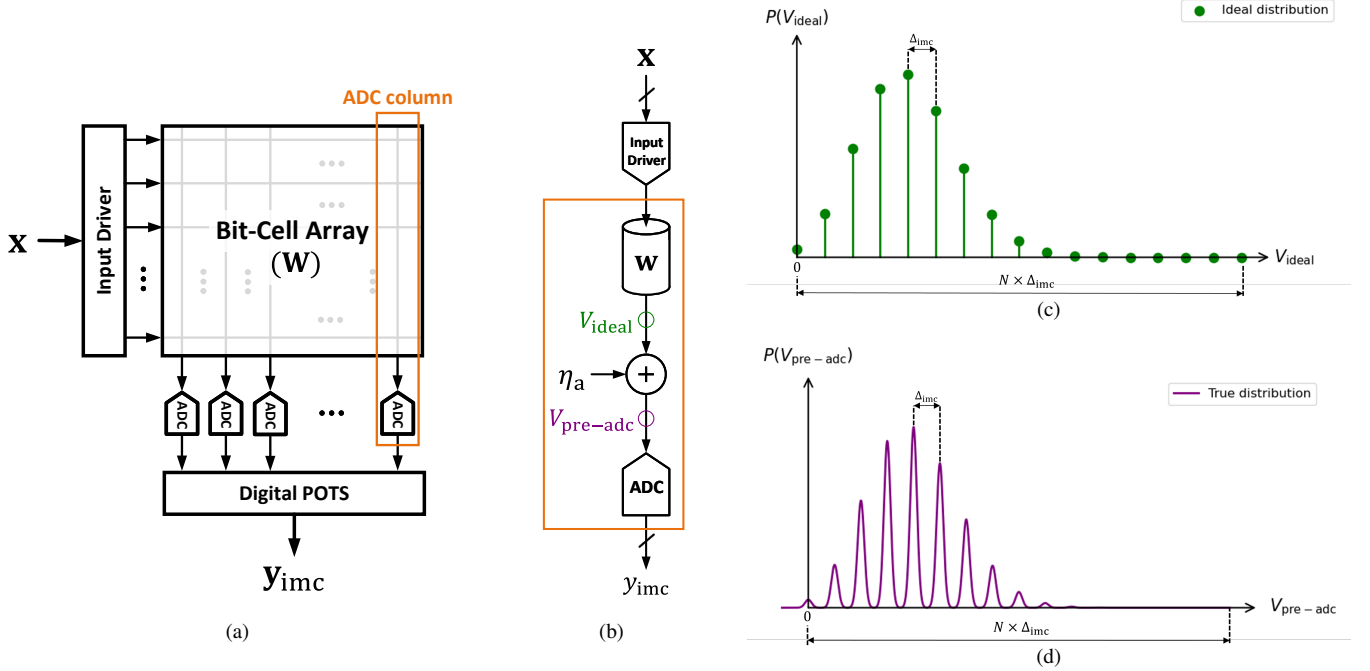


Fig. 2: AIMC used for computing an MVM: (a) components of an AIMC bank, (b) model of a dot product computation in an ADC column showing the ideal voltage-domain dot product (V_{ideal}), additive Gaussian noise (η_a), and pre-ADC signal ($V_{\text{pre-adc}}$). For a binary N -dimensional dot product: (c) V_{ideal} has a binomial distribution, and (d) $V_{\text{pre-adc}}$ has a Gaussian mixture distribution with inter-level spacing of Δ_{imc} .

the convergence rate of LM can be extremely slow. Finally, LM-based ADCs are non-uniform creating several implementation challenges as indicated earlier.

The optimal clipping criterion (OCC) [26] provides an implementation-friendly alternative to an LM quantizer. An OCC-based ADC employs uniformly-spaced quantization levels with the lowest (t_1) and highest (t_M) clipping levels chosen to maximize the SQNR. In doing so, it achieves an SQNR close to that of the theoretically-optimal LM-quantizer while being easy to implement. However, OCC assumes a Gaussian distributed ADC input and input-independent quantization noise like the other works.

In this paper, we will employ the full-range (FR), LM- and OCC-based ADCs as baselines to compare our CSNR-optimal ADCs against. Figure 3 shows the distinction between the three baselines and our proposed CSNR-optimal ADCs. Note: the CSNR-optimal ADC is also a uniform ADC. However, unlike the baselines, it accounts for the true ADC input distribution (Gaussian mixture) to set the quantization levels and thresholds. As a result, it can achieve a 8.4 dB higher CSNR than the best baseline in the example shown in Fig. 3.

Our work is inspired by [33], [34] where it was shown that ADCs that minimize the ultimate metric, bit-error rate (BER), of a communication link require less precision than conventional SQNR-optimal ADCs. However, unlike BER-optimal ADCs, our CSNR-optimal ADCs are uniform and therefore easy to implement in silicon, and target AIMCs.

C. CSNR: Accuracy Metric for AIMCs

Figure 2(a) shows the architecture of a standard AIMC bank comprising an input driver, bit-cell array (BCA), ADCs, and digital power-of-two-summation (POTS) logic to compute a dot product per ADC column as follows:

$$y_{\text{ideal}} = \mathbf{w}^T \mathbf{x} \quad (9)$$

where \mathbf{x} is the input vector, \mathbf{w} is a column vector of the weights, and y_{ideal} is the ideal dot product before POTS processing. Due to analog circuit non-idealities and quantization errors, the AIMC computation results in a computational error given by:

$$e(\mathbf{w}, \mathbf{x}) = y_{\text{imc}} - y_{\text{ideal}} \quad (10)$$

where y_{imc} is the AIMC-based dot product, and $e(\mathbf{w}, \mathbf{x})$ denotes the dot product computational error corresponding to \mathbf{w} and \mathbf{x} . The accuracy of the AIMC-based dot product computation is measured using the compute signal-to-noise ratio (CSNR), defined as:

$$\text{CSNR} = \frac{\text{Var}(y_{\text{ideal}})}{\text{Var}(e(\mathbf{w}, \mathbf{x}))} = \frac{\text{Var}(y_{\text{ideal}})}{\text{Var}(y_{\text{imc}} - y_{\text{ideal}})} \quad (11)$$

where \mathbf{w} and \mathbf{x} are random vectors representing the weight and input vectors, respectively, and y_{ideal} and y_{imc} are the random variables representing the ideal and AIMC-based dot product outputs, respectively. Since any constant offset in the AIMC-based dot product can be calibrated out digitally, we

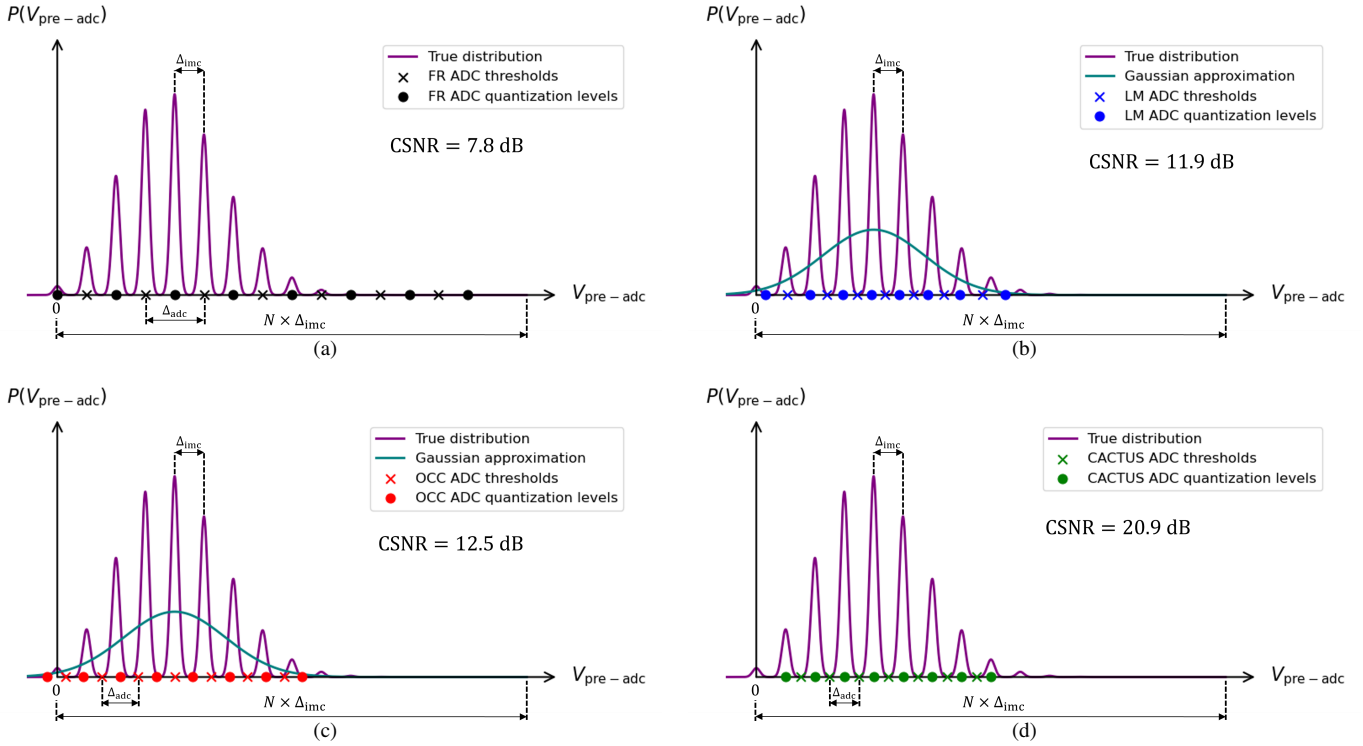


Fig. 3: Example of quantization thresholds of different types of column ADCs for $N = 16$, $\Delta_{imc} = 39.4$ mV, $\sigma_a = 5$ mV, and $B_{adc} = 3$ b: (a) full range (FR), (b) Lloyd-Max (LM), (c) optimal clipping criteria (OCC), and the (d) proposed CSNR-optimal ADC obtained from CACTUS. The CSNR values are obtained using Theorem 2 and its extensions.

assume $e(\mathbf{w}, \mathbf{x})$ to be zero mean and rewrite (11) as:

$$\text{CSNR} = \frac{\text{Var}(y_{\text{ideal}})}{\mathbb{E}[(y_{\text{imc}} - y_{\text{ideal}})^2]} = \frac{\text{Var}(y_{\text{ideal}})}{\text{MSE}_{\text{dp}}} \quad (12)$$

where MSE_{dp} is the mean squared dot product error.

CSNR is a task agnostic metric that quantifies the computational accuracy of AIMCs. In contrast, most prior works report only task specific metrics, such as classification accuracy in image classification tasks. However, such task specific metrics can make it difficult to compare different AIMC designs, as they are influenced by the algorithm mapped onto the AIMC. For instance, different machine learning models may yield different classification accuracies even when executed on the same AIMC. As a result, CSNR is slowly gaining broader adoption [13], [15], [35], [36] as the standard bank level metric for evaluating AIMC's computational accuracy. Some works [35], [36] refer to it as the compute signal-to-noise-plus-distortion ratio (CSNDR) to highlight the distortion effects introduced by circuit parasitics.

III. PROPOSED COMPUTE SNR-OPTIMAL ADCs

The AIMC-based dot product in (10) can be expressed as:

$$y_{\text{imc}} = \text{Dig}(Q_{\mathbf{t}, \mathbf{r}}(V_{\text{pre-adc}})) \quad (13)$$

where $V_{\text{pre-adc}}$ is the pre-ADC voltage-domain value of the AIMC dot product, $Q_{\mathbf{t}, \mathbf{r}}(\cdot)$ is the quantization function defined

in (2), and $\text{Dig}(\cdot)$ denotes the digital encoding function that maps the quantization levels to a digital representation (e.g., unsigned, two's complement, etc.). For a given B_{adc} , we define a CSNR-optimal ADC as the solution to the following optimization problem:

$$\begin{aligned} \{\mathbf{t}^\dagger, \mathbf{r}^\dagger\} &= \arg \max_{\mathbf{t}, \mathbf{r}} \text{CSNR} = \arg \min_{\mathbf{t}, \mathbf{r}} \text{MSE}_{\text{dp}} \\ &= \arg \min_{\mathbf{t}, \mathbf{r}} \mathbb{E}[(\text{Dig}(Q_{\mathbf{t}, \mathbf{r}}(V_{\text{pre-adc}})) - y_{\text{ideal}})^2] \end{aligned} \quad (14)$$

where \mathbf{t}^\dagger and \mathbf{r}^\dagger are the thresholds and quantization levels of the CSNR-optimal ADC, respectively.

A. Modeling and Analysis of AIMCs

To enable a direct mapping between the digital representation of dot product values and voltage-domain signals in AIMC, we assume y_{ideal} is an unsigned discrete random variable with a known probability mass function:

$$p_{y_{\text{ideal}}}(y) = \Pr\{y_{\text{ideal}} = y\}, \quad y_{\text{ideal}} \in \{0, 1, \dots, N\} \quad (15)$$

where $N \in \mathbb{N}$ is the maximum value of y_{ideal} . AIMCs computing binary N -dimensional dot products with Bernoulli distributed $\text{Be}(0.5)$ weights and inputs, result in $y_{\text{ideal}} \sim \text{Bi}(N, 0.25)$ with its voltage-domain equivalent given by:

$$V_{\text{ideal}} = y_{\text{ideal}} \times \Delta_{imc} \quad (16)$$

where V_{ideal} is a discrete random variable representing the ideal dot product in the voltage-domain, and Δ_{imc} is a fixed scaling factor.

The pre-ADC voltage is influenced by various circuit non-idealities and can be modeled as¹:

$$V_{\text{pre-adc}} = V_{\text{ideal}} + \eta_a, \quad \eta_a \sim \mathcal{N}(0, \sigma_a^2) \quad (17)$$

where η_a models thermal noise and charge injection. Fig. 2 illustrates an example of distributions of V_{ideal} and $V_{\text{pre-adc}}$ modeled as per (15)-(17).

We chose the digital encoding function in (13) such that when the voltage-domain quantization levels are scaled by Δ_{imc} in (16), the resulting fixed offset μ_{off} in the computational error is calibrated out, i.e., $\mathbb{E}[y_{\text{imc}} - y_{\text{ideal}}] = 0$. The resulting μ_{off} is given by:

$$\mu_{\text{off}} = \mathbb{E} \left[\frac{Q_{\mathbf{t}, \mathbf{r}}(y_{\text{ideal}} \times \Delta_{\text{imc}} + \eta_a) - y_{\text{ideal}}}{\Delta_{\text{imc}}} \right] \quad (18)$$

Thus, an AIMC is parametrized by: 1) N dot product levels, 2) $p_{y_{\text{ideal}}}$ distribution of ideal dot product, 3) Δ_{imc} scaling factor, 4) B_{adc} ADC precision, 5) σ_a standard deviation of analog circuit noise, 6) t_1 smallest ADC clipping threshold, and 7) t_M largest ADC clipping threshold. We denote this parameterization as: $\text{AIMC}(N, p_{y_{\text{ideal}}}, \Delta_{\text{imc}}, B_{\text{adc}}, \sigma_a, t_1, t_M)$.

We now derive analytical expressions for μ_{off} , MSE_{dp} and CSNR for AIMCs via Theorems 1 and 2.

Theorem 1. For an $\text{AIMC}(N, p_{y_{\text{ideal}}}, \Delta_{\text{imc}}, B_{\text{adc}}, \sigma_a, t_1, t_M)$ modeled via (15)–(17) with uniform ADCs modeled via (1)–(5), the μ_{off} in (18) is given by:

$$\mu_{\text{off}} = \frac{1}{\Delta_{\text{imc}}} \sum_{y=0}^N p_{y_{\text{ideal}}}(y) \left\{ r_M - y\Delta_{\text{imc}} - \Delta_{\text{adc}} \sum_{k=1}^M \Phi \left(\frac{t_k - y\Delta_{\text{imc}}}{\sigma_a} \right) \right\} \quad (19)$$

where,

$$\Phi(x) = \int_{-\infty}^x \frac{e^{-z^2/2}}{\sqrt{2\pi}} dz \quad \forall x \in \mathbb{R} \quad (20)$$

Proof: See Appendix.

Theorem 2. For an $\text{AIMC}(N, p_{y_{\text{ideal}}}, \Delta_{\text{imc}}, B_{\text{adc}}, \sigma_a, t_1, t_M)$ modeled via (15)–(17) with uniform ADCs modeled via (1)–(5), the MSE_{dp} and CSNR in (12) are given by:

$$\text{MSE}_{\text{dp}} = \alpha - \mu_{\text{off}}^2 \quad (21)$$

and

$$\text{CSNR} = \frac{\sum_{y=0}^N y^2 p_{y_{\text{ideal}}}(y) - \left(\sum_{y=0}^N y p_{y_{\text{ideal}}}(y) \right)^2}{\alpha - \mu_{\text{off}}^2} \quad (22)$$

¹Embedded non-volatile memory (eNVM)-based AIMCs may require more complex models to account for distortion due to eNVM device non-idealities and wire parasitics [35]. However, most state-of-the-art SRAM-based AIMCs are well-approximated by (17) [15], [25].

where,

$$\alpha = \frac{1}{\Delta_{\text{imc}}^2} \sum_{y=0}^N p_{y_{\text{ideal}}}(y) \left\{ (r_M - y\Delta_{\text{imc}})^2 - 2\Delta_{\text{adc}} \sum_{k=1}^M (t_k - y\Delta_{\text{imc}}) \Phi \left(\frac{t_k - y\Delta_{\text{imc}}}{\sigma_a} \right) \right\}, \quad (23)$$

μ_{off} is defined in (19) and $\Phi(\cdot)$ is defined in (20).

Proof: See Appendix.

B. Visualizing CSNR of AIMCs

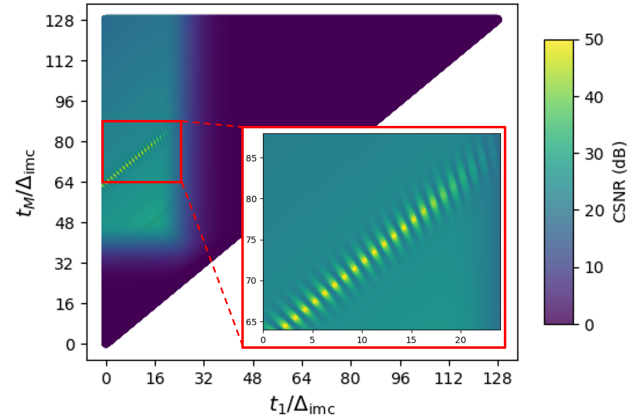


Fig. 4: Theoretical compute signal-to-noise ratio (CSNR) from Theorem 2 as a function of ADC clipping thresholds, assuming $y_{\text{ideal}} \sim \text{Bi}(128, 0.25)$, $\Delta_{\text{imc}} = 10 \times \sigma_a$, and $B_{\text{adc}} = 5$ b.

Based on an analysis of CSNR across a range of AIMC configurations (see Fig. 4 for a specific example), we make the following observations:

- 1) CSNR is a non-convex function of t_1 and t_M , with multiple local maxima.
- 2) CSNR exhibits large spikes at local maxima when $\Delta_{\text{imc}} \gg \sigma_a$.
- 3) These spikes occur when Δ_{adc} becomes an integer multiple of Δ_{imc} and the ADC quantization levels align with the high-probability levels of y_{ideal} .

Based on these observations, we propose an algorithm, CACTUS, to solve (14) under the constraint of uniform quantization.

C. CACTUS Algorithm

Algorithm 1 (CACTUS) estimates the CSNR-optimal clipping thresholds for uniform ADCs in AIMCs, for a given ADC precision, and provides estimates of the minimum achievable MSE_{dp} and the corresponding maximum CSNR. CACTUS first checks whether the ADC precision is sufficient to represent all N possible dot product values (i.e., if $B_{\text{adc}} \geq \log_2 N$). If so, it directly sets the clipping thresholds such that the quantization levels match the V_{ideal} levels, and estimates MSE_{dp} and CSNR using Theorem 2. Otherwise, CACTUS performs

Algorithm 1 CSNR-optimal ADC Clipping Thresholds Search (CACTUS)

```

1: Inputs:  $N$ ,  $p_{y_{\text{ideal}}}$ ,  $\Delta_{\text{imc}}$ ,  $B_{\text{adc}}$ ,  $\sigma_a$ 
2: Outputs:  $t_1^\dagger, t_M^\dagger, \text{MSE}_{\text{dp}}^{\min}, \text{CSNR}^{\max}$ 
3: if  $B_{\text{adc}} \geq \log_2 N$  then
4:    $t_1^\dagger \leftarrow 0.5\Delta_{\text{imc}}$ ,  $t_M^\dagger \leftarrow (M - 0.5)\Delta_{\text{imc}}$ 
5:    $\text{MSE}_{\text{dp}}^{\min}, \text{CSNR}^{\max} \leftarrow \text{Th. 2}$  with parameters:
         $(N, p_{y_{\text{ideal}}}, \Delta_{\text{imc}}, B_{\text{adc}}, \sigma_a, t_1^\dagger, t_M^\dagger)$ 
6:   return  $t_1^\dagger, t_M^\dagger, \text{MSE}_{\text{dp}}^{\min}, \text{CSNR}^{\min}$ 
7: else
8:    $t_1^\dagger, t_M^\dagger \leftarrow 0$ ,  $\text{MSE}_{\text{dp}}^{\min} \leftarrow \infty$ ,  $\text{CSNR}^{\max} \leftarrow -\infty$ ,
      $M \leftarrow 2^{B_{\text{adc}}} - 1$ ,  $k \leftarrow 1$ 
9:   while  $(M - 0.5)k < N$  do
10:     $\Delta_{\text{adc}} \leftarrow k\Delta_{\text{imc}}$ ,  $l \leftarrow 0$ 
11:    while  $(M - 1)k + l + 0.5 < N$  do
12:       $t'_1 \leftarrow (l + 0.5)\Delta_{\text{imc}}$ ,  $t'_M \leftarrow t'_1 + (M - 1)\Delta_{\text{adc}}$ 
13:       $\text{MSE}'_{\text{dp}}, \text{CSNR}' \leftarrow \text{Th. 2}$  with parameters:
           $(N, p_{y_{\text{ideal}}}, \Delta_{\text{imc}}, B_{\text{adc}}, \sigma_a, t'_1, t'_M)$ 
14:      if  $\text{MSE}'_{\text{dp}} < \text{MSE}_{\text{dp}}^{\min}$  then
15:         $t_1^\dagger, t_M^\dagger \leftarrow t'_1, t'_M$ 
16:         $\text{MSE}_{\text{dp}}^{\min}, \text{CSNR}^{\max} \leftarrow \text{MSE}'_{\text{dp}}, \text{CSNR}'$ 
17:      end if
18:       $l \leftarrow l + 1$ 
19:    end while
20:     $k \leftarrow k + 1$ 
21:  end while
22:  return  $t_1^\dagger, t_M^\dagger, \text{MSE}_{\text{dp}}^{\min}, \text{CSNR}^{\max}$ 
23: end if

```

an iterative search over a finite set of candidate threshold pairs that satisfy two conditions: 1) Δ_{adc} is an integer multiple of Δ_{imc} , and 2) each threshold lies exactly in between its two nearest V_{ideal} levels. For each candidate (t'_1, t'_M) , CACTUS estimates MSE_{dp} and CSNR using Theorem 2, and selects the candidate with the lowest MSE_{dp} .

Algorithm 2 determines the minimum ADC precision required to meet a target CSNR specification. At each iteration, the algorithm estimates the maximum achievable CSNR using CACTUS and increments the ADC precision B_{adc}^{\min} until the target $\text{CSNR}^{\text{spec}}$ is met.

IV. SIMULATION RESULTS

A. Simulation Setup

Figure 5 shows the simulation setup used to evaluate the CSNR of an SRAM-based AIMC. We build a circuit-aware behavioral model of an SRAM-based AIMC chip in a 28 nm CMOS process, based on (15)–(17), using post-layout simulation data from [37]. The model computes the value of Δ_{imc} in (16) based on the supply voltage, bit-cell capacitance, and

Algorithm 2 Minimum ADC precision requirement

```

1: Inputs:  $N$ ,  $p_{y_{\text{ideal}}}$ ,  $\Delta_{\text{imc}}$ ,  $\sigma_a$ ,  $\text{CSNR}^{\text{spec}}$ 
2: Output:  $B_{\text{adc}}^{\min}$ 
3:  $B_{\text{adc}}^{\min} \leftarrow 1$ 
4: while  $B_{\text{adc}}^{\min} \leq \lceil \log_2 N \rceil$  do
5:    $\text{CSNR}^{\max} \leftarrow \text{CACTUS } (N, p_{y_{\text{ideal}}}, \Delta_{\text{imc}}, B_{\text{adc}}^{\min}, \sigma_a)$ 
6:   if  $\text{CSNR}^{\max} \geq \text{CSNR}^{\text{spec}}$  then
7:     return  $B_{\text{adc}}^{\min}$ 
8:   else
9:      $B_{\text{adc}}^{\min} \leftarrow B_{\text{adc}}^{\min} + 1$ 
10:  end if
11: end while

```

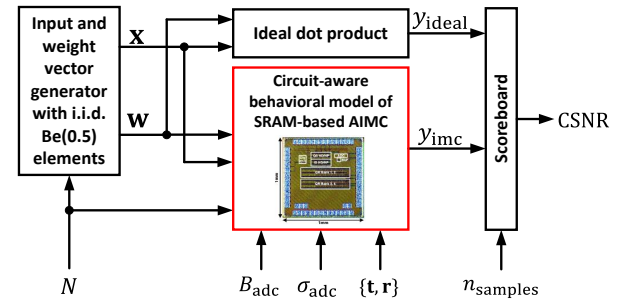


Fig. 5: Simulation setup for evaluating CSNR of an SRAM-based AIMC computing $y_{\text{ideal}} = \mathbf{w}^T \mathbf{x}$.

dot product dimension (N). It accounts for parasitic capacitance, bit-cell capacitance mismatch and models ADC thermal noise with variance σ_{adc} as the primary source of the additive Gaussian noise η_a in (17). We assume Be(0.5) weights and inputs, 0.9 V supply voltage, and 1 fF bit-cell capacitance. We present CSNR results for σ_{adc} values representative of practical SAR ADC designs [38]. We set $n_{\text{samples}} = 5 \times 10^5$ and report values of $\text{CSNR} \leq 50$ dB, as this corresponds to > 100 samples producing computational errors. Estimating CSNR above 50 dB would require significantly more samples, increasing simulation time. We share an anonymized repository containing our behavioral model and CSNR evaluation code: <https://github.com/mihirvk2/CSNR-optimal-ADC>.

B. Impact of N and σ_{adc} on $V_{\text{pre-adc}}$

Figure 6 illustrates the impact of dot product dimension (N) and ADC thermal noise standard deviation (σ_{adc}) on the pre-ADC voltage distribution ($V_{\text{pre-adc}}$). Assuming a Be(0.5) distribution for both inputs and weights, the ideal dot product follows $y_{\text{ideal}} \sim \text{Bi}(N, 0.25)$. As N increases, the distribution narrows due to the \sqrt{N} scaling of the standard deviation of a binomial random variable. For small N and σ_{adc} , the true distribution deviates significantly from a Gaussian. However, when $N \geq 256$ or $\sigma_{\text{adc}} \geq 0.75$ mV, the resulting Gaussian mixture approaches a Gaussian distribution. As expected and

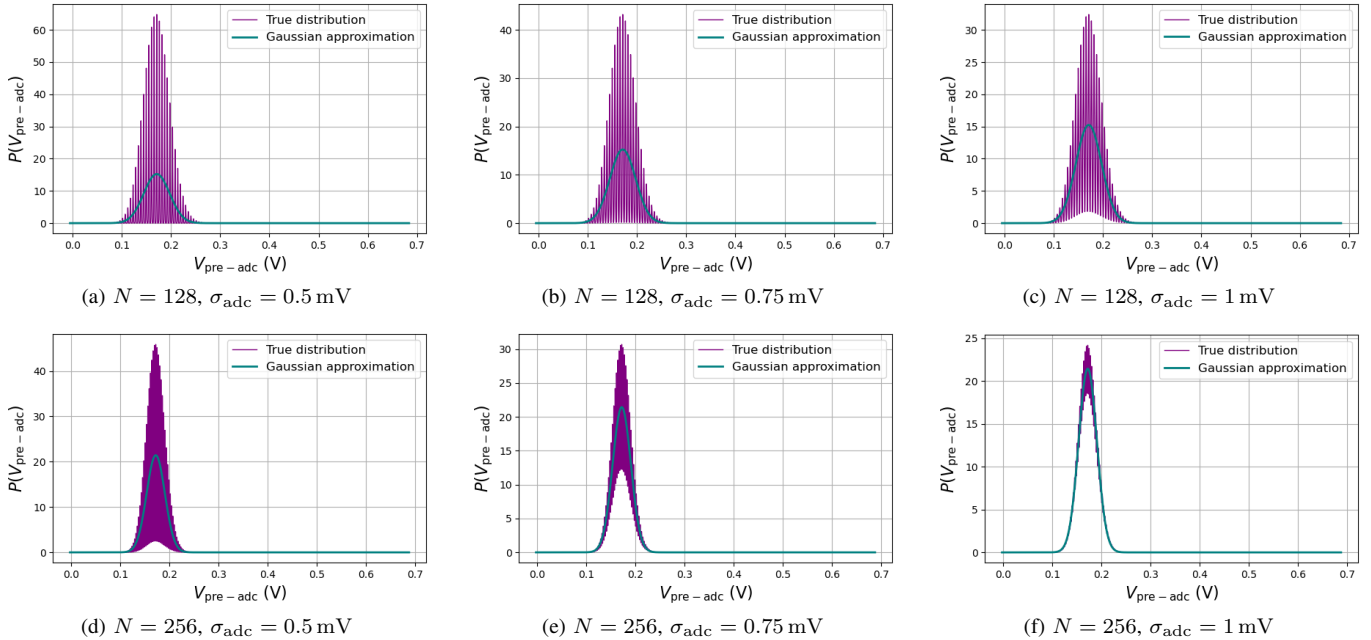


Fig. 6: Impact of dot product dimension (N) and standard deviation of ADC thermal noise (σ_{adc}) on the pre-ADC voltage ($V_{\text{pre-adc}}$) distribution.

shown later in Fig. 7, under these conditions, the gap between CSNR-optimal ADCs and SQNR-optimal ADCs reduces.

C. Impact of $\{t, r\}$ on CSNR

We compare the performance of a CACTUS ADC against the baseline ADCs illustrated in Fig. 3:

- 1) **Full range (FR):** In an FR uniform ADC, the clipping thresholds in (2) are given by:

$$\Delta_{\text{adc}} = \frac{N \Delta_{\text{imc}}}{M + 1} \quad (24)$$

$$t_1 = 0.5 \Delta_{\text{adc}}, \quad t_M = (M - 0.5) \Delta_{\text{adc}}$$

- 2) **Optimal clipping criterion (OCC):** In an OCC-based uniform ADC [26], the clipping thresholds are derived based on the assumption that the ADC input follows a Gaussian distribution. Thus we approximate the input as a Gaussian and apply OCC.
- 3) **Lloyd-Max (LM):** The LM algorithm [30], [31] can get trapped in local minima for multi-peak distributions, so we approximate the input as Gaussian for consistent results.

Figure 7 shows that CACTUS consistently outperforms the FR, LM, and OCC baselines across various operating conditions. We see that CACTUS can provide > 20 dB gain in CSNR at a given ADC precision, reduce the ADC precision requirement by > 4 b to meet a target CSNR, and achieve around 6 dB CSNR improvement while simultaneously saving 3 b in ADC precision. These benefits diminish as N and σ_{adc} increase, as ADC noise becomes dominant due to a reduced $\Delta_{\text{imc}}/\sigma_{\text{adc}}$ ratio, causing the CSNR- and SQNR-optimal ADC designs to converge. We also observe a CSNR peak

in FR ADC at $B_{\text{adc}} = \log_2 N$, where it behaves identically to CACTUS. In this regime, AIMC can achieve a CSNR significantly higher than the ADC's SQNR, as quantizing $V_{\text{pre-adc}}$ to V_{ideal} can cancel the analog noise (η_a). This peaking contradicts prior assertions [25] that CSNR should increase with SQNR and is upper bounded by it, but is explained by the theoretical analysis in this paper.

Figure 7 also shows that the simulation results closely match the theoretical predictions of Theorem 2 (dashed lines) and its extensions.

V. CONCLUSION

This paper challenges conventional assumptions about the ADC's role in an AIMC and motivates the exploration of alternative design methodologies that directly optimize for AIMC's CSNR rather than ADC's SQNR. We propose one such method, based on the theoretical analysis of CSNR-optimal uniform ADCs for AIMCs, and demonstrate its energy and accuracy benefits. The underlying mathematical framework is general enough to support the development of other approaches. More broadly, this work encourages investigation into application-specific ADC designs, where task knowledge can help identify the ADC's true role at the system level and enable more efficient design optimizations.

APPENDIX

Proof of Theorem 1: For a fixed y , the probability mass function of $Q_{t,r}(y \Delta_{\text{imc}} + \eta_a)$ can be written using (2) as

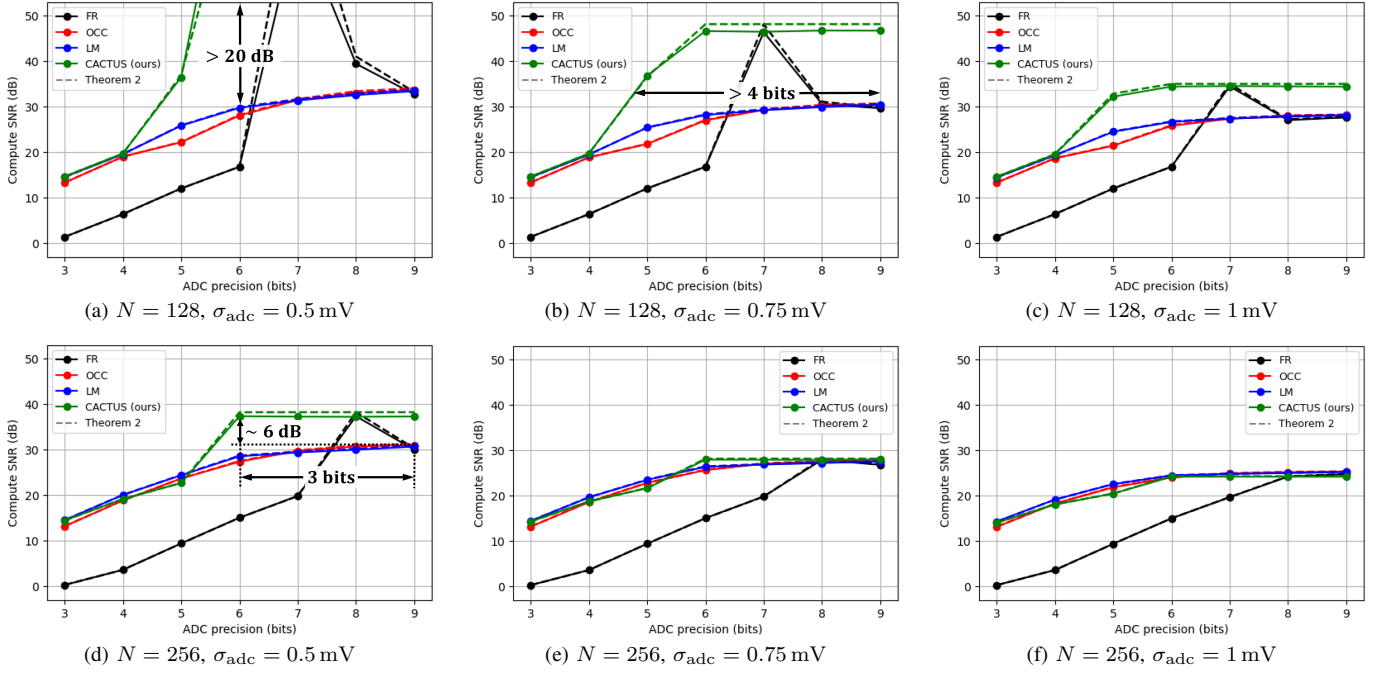


Fig. 7: Impact of ADC quantization scheme on the accuracy of SRAM-based AIMC for different dot product dimensions (N) and standard deviations of ADC thermal noise (σ_{adc}).

follows:

$$\Pr(Q_{\mathbf{t},\mathbf{r}}(y\Delta_{\text{imc}} + \eta_a) = r_k) = \begin{cases} \Phi\left(\frac{t_1 - y\Delta_{\text{imc}}}{\sigma_a}\right) & , \text{ if } k = 0 \\ \Phi\left(\frac{t_{k+1} - y\Delta_{\text{imc}}}{\sigma_a}\right) - \Phi\left(\frac{t_k - y\Delta_{\text{imc}}}{\sigma_a}\right) & , \text{ if } k \in \{1, 2, \dots, M-1\} \\ 1 - \Phi\left(\frac{t_M - y\Delta_{\text{imc}}}{\sigma_a}\right) & , \text{ if } k = M \end{cases} \quad (25)$$

where $\Phi(\cdot)$ is expressed in (20). We use (25) to derive:

$$\mathbb{E}_{\eta_a} [Q_{\mathbf{t},\mathbf{r}}(y_{\text{ideal}}\Delta_{\text{imc}} + \eta_a)] = r_M - \Delta_{\text{adc}} \sum_{k=1}^M \Phi\left(\frac{t_k - y_{\text{ideal}}\Delta_{\text{imc}}}{\sigma_a}\right) \quad (26)$$

Using the tower property of conditional expectation, we can write:

$$\mathbb{E}[y_{\text{imc}}] = \mathbb{E}_{y_{\text{ideal}}} [\mathbb{E}_{\eta_a} [y_{\text{imc}} | y_{\text{ideal}}]] \quad (27)$$

We use (26) and $p_{y_{\text{ideal}}}$ to evaluate the inner and outer expectations in (27), respectively, and substitute the result into (18) to obtain the expression in Theorem 1.

Proof of Theorem 2: We express MSE_{dp} as,

$$\mathbb{E}[(y_{\text{imc}} - y_{\text{ideal}})^2] = \frac{\mathbb{E}[(Q_{\mathbf{t},\mathbf{r}}(y_{\text{ideal}}\Delta_{\text{imc}} + \eta_a))^2]}{\Delta_{\text{imc}}^2} - \frac{2\mathbb{E}[y_{\text{ideal}}Q_{\mathbf{t},\mathbf{r}}(y_{\text{ideal}}\Delta_{\text{imc}} + \eta_a)]}{\Delta_{\text{imc}}} + \mathbb{E}[y_{\text{ideal}}^2] - \mu_{\text{off}}^2 \quad (28)$$

We use (25) to derive:

$$\begin{aligned} \mathbb{E}_{\eta_a} [(Q_{\mathbf{t},\mathbf{r}}(y_{\text{ideal}}\Delta_{\text{imc}} + \eta_a))^2] &= r_M^2 - 2\Delta_{\text{adc}} \sum_{k=1}^M t_k \Phi\left(\frac{t_k - y_{\text{ideal}}\Delta_{\text{imc}}}{\sigma_a}\right) \end{aligned} \quad (29)$$

Using the tower property of conditional expectation, we can write:

$$\mathbb{E}[(y_{\text{imc}} - y_{\text{ideal}})^2] = \mathbb{E}_{y_{\text{ideal}}} [\mathbb{E}_{\eta_a} [(y_{\text{imc}} - y_{\text{ideal}})^2 | y_{\text{ideal}}]] \quad (30)$$

We use (26), (29), and $p_{y_{\text{ideal}}}$ to evaluate the inner and outer expectations in (30), respectively, and substitute the result into (28) to obtain the expression in Theorem 2.

REFERENCES

- [1] N. Verma, H. Jia, H. Valavi, Y. Tang, M. Ozatay, L.-Y. Chen, B. Zhang, and P. Deaville, "In-memory computing: Advances and prospects," *IEEE Solid-State Circuits Magazine*, vol. 11, no. 3, pp. 43–55, 2019.
- [2] A. Sebastian, M. Le Gallo, R. Khaddam-Aljameh, and E. Eleftheriou, "Memory devices and applications for in-memory computing," *Nature nanotechnology*, vol. 15, no. 7, pp. 529–544, 2020.

[3] N. R. Shanbhag and S. K. Roy, "Benchmarking in-memory computing architectures," *IEEE Open Journal of the Solid-State Circuits Society*, vol. 2, pp. 288–300, 2022.

[4] J. Sun, P. Houshmand, and M. Verhelst, "Analog or digital in-memory computing? benchmarking through quantitative modeling," in *2023 IEEE/ACM International Conference on Computer Aided Design (ICCAD)*, 2023, pp. 1–9.

[5] Q. Dong, M. E. Sinangil, B. Erbagci, D. Sun, W.-S. Khwa, H.-J. Liao, Y. Wang, and J. Chang, "15.3 a 351tops/w and 372.4gops compute-in-memory sram macro in 7nm finfet cmos for machine-learning applications," in *IEEE International Solid-State Circuits Conference - (ISSCC)*, 2020, pp. 242–244.

[6] H. Jia, H. Valavi, Y. Tang, J. Zhang, and N. Verma, "A programmable heterogeneous microprocessor based on bit-scalable in-memory computing," *IEEE Journal of Solid-State Circuits*, vol. 55, no. 9, pp. 2609–2621, 2020.

[7] Z. Jiang, S. Yin, J.-S. Seo, and M. Seok, "C3sram: An in-memory computing sram macro based on robust capacitive coupling computing mechanism," *IEEE Journal of Solid-State Circuits*, vol. 55, no. 7, pp. 1888–1897, 2020.

[8] I. A. Papistas, S. Cosemans, B. Rooseleer, J. Doevespeck, M.-H. Na, A. Mallik, P. Debacker, and D. Verkest, "A 22 nm, 1540 top/s/w, 12.1 top/mm² in-memory analog matrix-vector-multiplier for dnn acceleration," in *2021 IEEE Custom Integrated Circuits Conference (CICC)*, 2021, pp. 1–2.

[9] J. Lee, H. Valavi, Y. Tang, and N. Verma, "Fully row/column-parallel in-memory computing sram macro employing capacitor-based mixed-signal computation with 5-b inputs," in *2021 Symposium on VLSI Circuits*, 2021, pp. 1–2.

[10] E. Choi, I. Choi, C. Jeon, G. Yun, D. Yi, S. Ha, I.-J. Chang, and M. Je, "A 133.6tops/w compute-in-memory sram macro with fully parallel one-step multi-bit computation," in *2022 IEEE Custom Integrated Circuits Conference (CICC)*, 2022, pp. 1–2.

[11] R. Sehgal, T. Thareja, S. Xie, C. Ni, and J. P. Kulkarni, "A bit-serial, compute-in-sram design featuring hybrid-integrating adcs and input dependent binary scaled precharge eliminating dacs for energy-efficient dnn inference," *IEEE Journal of Solid-State Circuits*, vol. 58, no. 7, pp. 2109–2124, 2023.

[12] H. Wang, R. Liu, R. Dorrance, D. Dasalukunte, D. Lake, and B. Carlton, "A charge domain sram compute-in-memory macro with c-2c ladder-based 8-bit mac unit in 22-nm finfet process for edge inference," *IEEE Journal of Solid-State Circuits*, vol. 58, no. 4, pp. 1037–1050, 2023.

[13] J. Lee, B. Zhang, and N. Verma, "A switched-capacitor sram in-memory computing macro with high-precision, high-efficiency differential architecture," in *2024 IEEE European Solid-State Electronics Research Conference (ESSERC)*, 2024, pp. 357–360.

[14] B. Choi, E. Choi, D. Yi, J. Chun, S. Ha, I.-J. Chang, and M. Je, "Ar-cim: A 460.22tops/w sram-based analog reconfigurable computing-in-memory macro with 1/2/4/8-bit variable precision," in *2024 IEEE European Solid-State Electronics Research Conference (ESSERC)*, 2024, pp. 361–364.

[15] K. Yoshioka, "A 818–4094 tops/w capacitor-reconfigured analog cim for unified acceleration of cnns and transformers," *IEEE Journal of Solid-State Circuits*, pp. 1–12, 2024.

[16] B. Zhang, J. Saikia, J. Meng, D. Wang, S. Kwon, S. Myung, H. Kim, S. J. Kim, J.-S. Seo, and M. Seok, "Macc-sram: A multistep accumulation capacitor-coupling in-memory computing sram macro for deep convolutional neural networks," *IEEE Journal of Solid-State Circuits*, vol. 59, no. 6, pp. 1938–1949, 2024.

[17] J. M. Correll, L. Jie, S. Song, S. Lee, J. Zhu, W. Tang, L. Wormald, J. Erhardt, N. Breil, R. Quon, D. Kamalanathan, S. Krishnan, M. Chudzik, Z. Zhang, W. D. Lu, and M. P. Flynn, "An 8-bit 20.7 tops/w multi-level cell reram-based compute engine," in *2022 IEEE Symposium on VLSI Technology and Circuits (VLSI Technology and Circuits)*, 2022, pp. 264–265.

[18] E. Choi, I. Choi, V. Lukito, D.-H. Choi, D. Yi, I.-J. Chang, S. Ha, and M. Je, "A 333tops/w logic-compatible multi-level embedded flash compute-in-memory macro with dual-slope computation," in *2023 IEEE Custom Integrated Circuits Conference (CICC)*, 2023, pp. 1–2.

[19] J.-M. Hung, T.-H. Wen, Y.-H. Huang, S.-P. Huang, F.-C. Chang, C.-I. Su, W.-S. Khwa, C.-C. Lo, R.-S. Liu, C.-C. Hsieh, K.-T. Tang, Y.-D. Chih, T.-Y. J. Chang, and M.-F. Chang, "8-b precision 8-mb reram compute-in-memory macro using direct-current-free time-domain readout scheme for ai edge devices," *IEEE Journal of Solid-State Circuits*, vol. 58, no. 1, pp. 303–315, 2023.

[20] S. D. Spetnick, M. Chang, S. Konno, B. Crafton, A. S. Lele, W.-S. Khwa, Y.-D. Chih, M.-F. Chang, and A. Raychowdhury, "A 40-nm compute-in-memory macro with rram addressing ir drop and off-state current," *IEEE Solid-State Circuits Letters*, vol. 7, pp. 10–13, 2024.

[21] P. Yao, Q. Wei, D. Wu, B. Gao, S. Yang, T.-Y. Shen, Q. Zhang, S. Pan, J. Tang, H. Qian, L. Jie, and H. Wu, "A 28 nm rram-based 81.1 tops/mm²/bit compute-in-memory macro with uniform and linear 64 read channels under 512 4-bit inputs," in *2024 IEEE European Solid-State Electronics Research Conference (ESSERC)*, 2024, pp. 577–580.

[22] J. von Neumann, "First draft of a report on the edvac," *IEEE Annals of the History of Computing*, vol. 15, no. 4, pp. 27–75, 1993.

[23] M. Horowitz, "1.1 computing's energy problem (and what we can do about it)," in *IEEE International Solid-State Circuits Conference Digest of Technical Papers (ISSCC)*, 2014, pp. 10–14.

[24] B. Murmann, "ADC Performance Survey 1997-2024," [Online]. Available: <https://github.com/bmurm/ADC-survey>.

[25] S. K. Gonugondla, C. Sakr, H. Dbouk, and N. R. Shanbhag, "Fundamental limits on the precision of in-memory architectures," in *IEEE/ACM International Conference On Computer Aided Design (ICCAD)*, 2020, pp. 1–9.

[26] C. Sakr and N. R. Shanbhag, "Signal processing methods to enhance the energy efficiency of in-memory computing architectures," *IEEE Transactions on Signal Processing*, vol. 69, pp. 6462–6472, 2021.

[27] B. Murmann, "Mixed-signal computing for deep neural network inference," *IEEE Transactions on Very Large Scale Integration (VLSI) Systems*, vol. 29, no. 1, pp. 3–13, 2021.

[28] K. He, I. Chakraborty, C. Wang, and K. Roy, "Design space and memory technology co-exploration for in-memory computing based machine learning accelerators," in *2022 IEEE/ACM International Conference On Computer Aided Design (ICCAD)*, 2022, pp. 1–9.

[29] A. B. Sundar, J. Viraghavan, and B. Vijayakumar, "Input-conditioned quantisation for enob improvement in cim adc columns targeting large-length partial sums," *IEEE Transactions on Circuits and Systems II: Express Briefs*, vol. 71, no. 6, pp. 2971–2975, 2024.

[30] S. Lloyd, "Least squares quantization in pcm," *IEEE Transactions on Information Theory*, vol. 28, no. 2, pp. 129–137, 1982.

[31] J. Max, "Quantizing for minimum distortion," *IRE Transactions on Information Theory*, vol. 6, no. 1, pp. 7–12, 1960.

[32] Y. Lu and H. H. Zhou, "Statistical and computational guarantees of lloyd's algorithm and its variants," 2016. [Online]. Available: <https://arxiv.org/abs/1612.02099>

[33] R. Narasimha, M. Lu, N. R. Shanbhag, and A. C. Singer, "Ber-optimal analog-to-digital converters for communication links," *IEEE Transactions on Signal Processing*, vol. 60, no. 7, pp. 3683–3691, 2012.

[34] Y. Lin, M.-S. Keel, A. Faust, A. Xu, N. R. Shanbhag, E. Rosenbaum, and A. C. Singer, "A study of ber-optimal adc-based receiver for serial links," *IEEE Transactions on Circuits and Systems I: Regular Papers*, vol. 63, no. 5, pp. 693–704, 2016.

[35] S. K. Roy and N. R. Shanbhag, "Energy-accuracy trade-offs for resistive in-memory computing architectures," *IEEE Journal on Exploratory Solid-State Computational Devices and Circuits*, vol. 10, pp. 22–30, 2024.

[36] S. K. Roy, H.-M. Ou, M. G. Ahmed, P. Deaville, B. Zhang, N. Verma, P. K. Hanumolu, and N. R. Shanbhag, "Compute snrd-boosted 22-nm mram-based in-memory computing macro using statistical error compensation," *IEEE Journal of Solid-State Circuits*, vol. 60, no. 3, pp. 1092–1102, 2025.

[37] S. Ji, "Analysis of the energy vs. accuracy tradeoff in the 10t1c bitcell-based in-memory architecture," Senior Thesis, University of Illinois Urbana-Champaign, May 2023. [Online]. Available: <https://hdl.handle.net/2142/124806>

[38] W. P. Zhang and X. Tong, "Noise modeling and analysis of sar adcs," *IEEE Transactions on Very Large Scale Integration (VLSI) Systems*, vol. 23, no. 12, pp. 2922–2930, 2015.